Joint full-waveform inversion of time-lapse seismic data sets

Musa Maharramov and Biondo Biondi

ABSTRACT

We present a technique for reconstructing subsurface model changes from time-lapse seismic survey data using full-waveform inversion (FWI). The technique is based on simultaneously inverting multiple survey vintages, with regularization of the model difference. In addition to the fully simultaneous FWI that requires the solution of a larger optimization problem, we propose a simplified cross-updating workflow that can be implemented using the existing FWI tools. The methods are demonstrated on synthetic examples, and their robustness with regard to repeatability issues is compared to alternative techniques, such as parallel, sequential, and double-difference methods.

INTRODUCTION

Effective reservoir monitoring depends on successful tracking of production-induced fluid movement in the reservoir and overburden, using input from seismic imaging, geomechanics, geology and reservoir simulation (Biondi et al., 1996). To achieve this, most traditional methods rely on the conversion of picked time shifts and reflectivity differences between migrated images into reflector movement and impedance changes. Though effective in practical applications, this approach requires a significant amount of expert interpretation and relies on quality control in the conversion process. Wave-equation image-difference tomography has been proposed as a more automatic alternative method to recover velocity changes (Albertin et al., 2006); it allows localized target-oriented inversion of model perturbations (Maharramov and Albertin, 2007). An alternative approach is based on using the high-resolution power of the full-waveform inversion (Sirgue et al., 2010) to reconstruct production-induced changes from wide-offset seismic acquisitions, and is the subject of this paper.

Time-lapse full-waveform inversion (Watanabe et al., 2004; Denli and Huang, 2009; Routh et al., 2012) is a promising technique for time-lapse seismic imaging where production-induced subsurface model changes are within the resolution of FWI. However, as with alternative time-lapse techniques, time-lapse FWI is sensitive to repeatability issues (Asnaashari et al., 2012). Non-repeatable acquisition geometries (e.g., slightly shifted source and receiver positions), acquisition gaps (e.g., due to new obstacles), different source signatures and measurement noise—all contribute to differences in the data from different survey vintages. Differences in the input data sets

due to repeatability issues may easily mask valuable production-induced changes. However, even with noise-free synthetic data without any acquisition repeatability issues, numerical artifacts may contaminate the inverted difference of monitor and baseline when practical limitations are imposed on solver iteration count. Maharramov and Biondi (2013) devised a time-lapse FWI that minimized model differences outside of areas affected by production by jointly inverting for multiple models, and imposing a regularization condition on the model difference. The joint inversion can be performed simultaneously for multiple model vintages or using an empirical technique of "cross-updating" (Maharramov and Biondi, 2013). In this work we apply these methods to noisy synthetic data and compare the results to alternative methods.

THE METHOD

Full-waveform inversion is defined as solving the following optimization problem (Tarantola, 1984; Virieux and Operto, 2009)

$$\|\mathbf{Mu} - \mathbf{d}\| \ \rightarrow \ \min \tag{1}$$

where $\mathbf{M}, \mathbf{d}$ are the measurement operator and data, $\mathbf{u}$ is the solution of a forward-modeling problem

$$\mathbf{D}(\mathbf{m})\mathbf{u} \ = \ \phi, \tag{2}$$

where $\mathbf{D}$ is the forward-modeling operator that depends on a model vector $\mathbf{m}$ as a parameter, and ϕ is a source. The minimization problem (1) is solved with respect to either both the model $\mathbf{m}$ and source ϕ or just the model. In the frequency-domain formulation of the acoustic waveform inversion, the forward-modeling equation (2) becomes

$$-\omega^2 u - v^2(x^1, \ldots, x^n)\Delta u \ = \ \phi(\omega, x^1, \ldots, x^n) \tag{3}$$

where ω is a temporal frequency, n is the problem dimension, and v is the acoustic wave propagation velocity. Values of the slowness $s = 1/v$ at all the points of the modeling domain constitute the model parameter vector $\mathbf{m}$. The direct problem (3) can be solved in the frequency domain, or in the time domain followed by a discrete Fourier transform in time (Virieux and Operto, 2009). The inverse problem (1) is typically solved using a multiscale approach, from low to high frequencies, supplying the output of each frequency inversion to the next step.

FWI applications in time-lapse problems seek to recover induced changes in the subsurface model using multiple data sets from different acquisition vintages. For two surveys sufficiently separated in time, we call such data sets (and the associated models) *baseline* and *monitor*.

Time-lapse FWI can be carried out by separately inverting the baseline and monitor models (*parallel difference*) or inverting them sequentially with, e.g., the baseline supplied as a starting model for the monitor inversion (*sequential difference*). Another

alternative is to apply the *double-difference* method, with a baseline model inversion followed by a monitor inversion that solves the following optimization problem

$$\| \left(\mathbf{M}_m^s \mathbf{u}_m - \mathbf{M}_b^s \mathbf{u}_b\right) - \left(\mathbf{M}_m \mathbf{d}_m - \mathbf{M}_b \mathbf{d}_b\right) \| \;\rightarrow\; \min \tag{4}$$

by changing the monitor model (Watanabe et al., 2004; Denli and Huang, 2009; Zheng et al., 2011; Asnaashari et al., 2012; Raknes et al., 2013). The subscripts in equation (4) denote the baseline and monitor surveys, $\mathbf{d}$ denotes the field data, and the $\mathbf{M}$'s are measurement operators that project the synthetic and field data onto a common grid. The superscript s indicates the measurement operators applied to the synthetic data.

In all of these techniques, optimization is carried out with respect to one model at a time, albeit of different vintages at different stages of the inversion. In our method we invert for the baseline and monitor models *simultaneously* by solving the following optimization problem:

$$\alpha \|\mathbf{M}_b \mathbf{u}_b - \mathbf{d}_b\|^2 + \beta \|\mathbf{M}_m \mathbf{u}_m - \mathbf{d}_m\|^2 + \tag{5}$$

$$\gamma \| \left(\mathbf{M}_m^s \mathbf{u}_m - \mathbf{M}_b^s \mathbf{u}_b\right) - \left(\mathbf{M}_m \mathbf{d}_m - \mathbf{M}_b \mathbf{d}_b\right) \|^2 + \tag{6}$$

$$\alpha_1 \|\mathbf{W}_b \mathbf{R}_b (\mathbf{m}_b - \mathbf{m}_b^{\text{PRIOR}})\|^2 + \tag{7}$$

$$\beta_1 \|\mathbf{W}_m \mathbf{R}_m (\mathbf{m}_m - \mathbf{m}_m^{\text{PRIOR}})\|^2 + \tag{8}$$

$$\delta \|\mathbf{W}\mathbf{R}(\mathbf{m}_m - \mathbf{m}_b - \Delta\mathbf{m}^{\text{PRIOR}})\|^2 \;\rightarrow\; \min, \tag{9}$$

with respect to both the baseline and monitor models $\mathbf{m}_b$ and $\mathbf{m}_m$. The terms (5) correspond to separate baseline and monitor inversions, the term (6) is the optional double difference term, the terms (7) and (8) are optional separate baseline and monitor inversion Tikhonov regularization terms (Aster et al., 2012), and the term (9) represents Tikhonov regularization of the model difference. In (7)-(9), $\mathbf{R}$ and $\mathbf{W}$ denote regularization and weighting operators respectively, with the subscript denoting the survey vintage where applicable.

A joint inversion approach has been applied earlier to the linearized waveform inversion (Ayeni and Biondi, 2012). In this work, we propose a simultaneous full-waveform inversion with special emphasis on regularization of the model difference in equation (9). Constraining the model difference where production effects are expected to be negligible while simultaneously solving for both baseline and monitor models can be expected to reduce both spurious numerical artifacts and non-repeatable acquisition-related artifacts in the model difference.

An implementation of the proposed simultaneous inversion algorithm requires solving a nonlinear optimization problem with twice the data and model dimensions of problems (1) and (4). The model difference regularization weights $\mathbf{W}$ and, optionally, the prior $\Delta\mathbf{m}^{\text{PRIOR}}$ may be obtained from prior geomechanical information. For example, a rough estimate of production-induced velocity changes can be obtained from time shifts (Hatchell and Bourne, 2005; Barkved and Kristiansen, 2005) and used to map subsurface regions of expected production-induced perturbation, and optionally provide a difference prior.

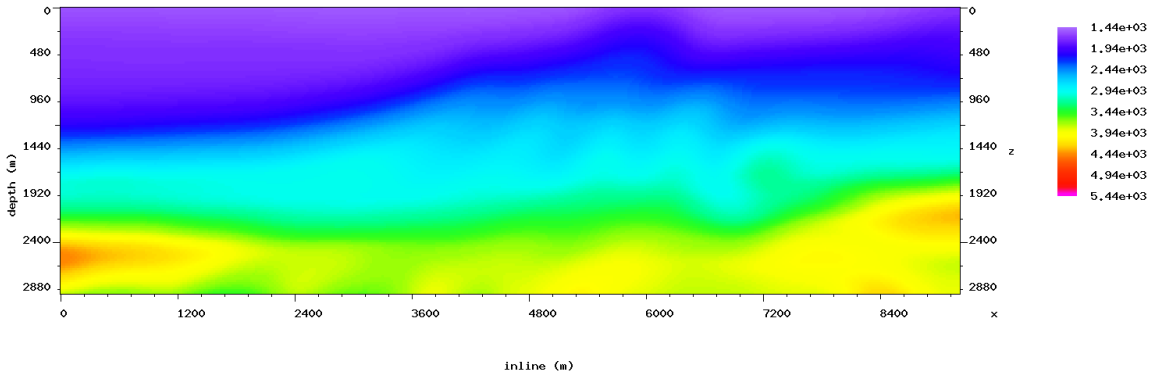

Figure 1: Starting model used in the inversion. [**CR**]

In addition to the fully simultaneous inversion, we propose a *cross-updating* technique that offers a simple but remarkably effective approximation to minimizing the objective function (5),(9), while obviating the difference regularization and weighting operators $\mathbf{R}$ and $\mathbf{W}$. This technique consists of one standard run of the sequential difference algorithm, followed by a second run with the inverted monitor model supplied as the starting model for the second baseline inversion

$$\begin{aligned} \mathbf{m}_{\text{INIT}} \rightarrow &\text{baseline inversion} \rightarrow \text{monitor inversion} \rightarrow \\ &\text{baseline inversion} \rightarrow \text{monitor inversion}, \end{aligned} \tag{10}$$

and computing the difference of the latest inverted monitor and baseline models. Process (10) can be considered as an approximation to minimizing (5) and (9) because non-repeatable footprints of both inversions are propagated to both models, canceling out in the difference. Both the simultaneous inversion and cross-updating minimize the model difference by tackling model artifacts that are in the null space of the Fréchet derivative of the forward modeling operator. The joint inversion minimizes the effect of such artifacts on the model difference by either minimizing the model difference term (9) in the simultaneous inversion, or by propagating these artifacts to both models in cross-updating (10). Note that this process is not guaranteed to improve the results of the baseline and monitor model inversions but is only proposed for improving the model difference.

NUMERICAL EXAMPLES

The Marmousi velocity model is used as a baseline, over a 384×122 grid with a 24 m grid spacing. Production-induced velocity changes are modeled as a negative −200 m/s perturbation at about 4.5 km inline 800 m depth, and a positive 300 m/s perturbation at 6.5 km inline, 1 km depth shown in Figure 4(a). The whole Marmousi model is inverted, however, only model differences for the section between the approximate inline coordinates 3.6 km and 7.2 km to the depth of approximately

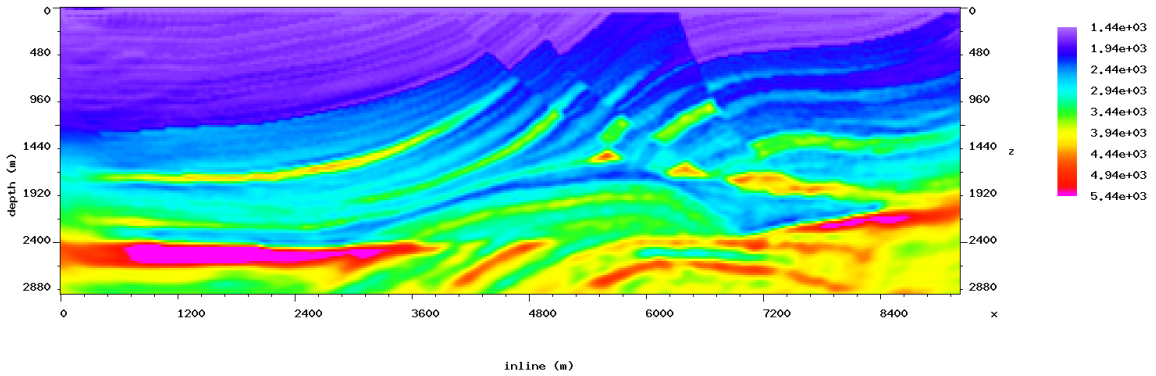

Figure 2: Baseline model inverted from noise-free synthetic data. [**CR**]

1.6 km are shown here. The inversion is carried out in the frequency domain for 3.0, 3.6, 4.3, 5.1, 6.2, 7.5, 9.0, 10.8, 12.8, and 15.5 Hz, where the frequencies are chosen based on the estimated offset to depth range of the data (Sirgue and Pratt, 2004). The baseline acquisition has 192 shots at a depth of 16 m with a 48 m spacing, and 381 receivers at a depth of 15 m with a 24 m spacing. The minimum offset is 48 m. The source function is a Ricker wavelet centered at 10.1 Hz. Absorbing boundary conditions are applied along the entire model boundary, including the surface (thus suppressing multiples). A smoothed true model (Figure 1) is used as a starting model for the initial baseline inversion (and for the initial monitor inversion in the parallel difference). The smoothing is performed using a triangular filter with a 20-sample half-window in both vertical and horizontal directions. The result of inverting the baseline model from the clean synthetic data is shown in Figure 2. Random Gaussian noise is added to the noise-free synthetic data to produce noisy data sets with 14 dB and 7 dB signal-to-noise ratios. Noisy monitor data sets are generated for the model perturbation of Figure 4(a), using the same acquisition geometry and source wavelet. The results of baseline model inversion from the 14 dB and 7 dB SNR synthetic data are shown in Figure 3(a) and Figure 3(b), respectively. Results of model difference inversion from the 14 dB and 7 dB SNR synthetic data sets using various methods are shown in Figures 5 and 6, respectively. The simultaneous inversion objective function contains only terms (5) and (9) with no difference prior, i.e., $\Delta\mathbf{m}^{\text{PRIOR}} = 0$. The model-difference regularization weights $\mathbf{W}$ in (9) are set to 1 outside approximately .5 km from the centers of the velocity anomalies (Figure 4(a)), tapering to zero within a smaller radius of the anomalies. The two terms in (5) are of the same magnitude and therefore α and β are set to 1. Parameter δ is set to 10^{-5} but can be varied for different acquisition source and geometry parameters. The result of the initial baseline inversion is supplied as a starting model for both $\mathbf{m}_b$ and $\mathbf{m}_m$ in the simultaneous inversion. In all the inversions, up to 10 iterations of the nonlinear conjugate gradients algorithm (Nocedal and Wright, 2006) are performed for each frequency. Neither regularization nor model priors are used in single-model inversions (i.e., in the cross-updating, parallel, sequential, and double difference methods).

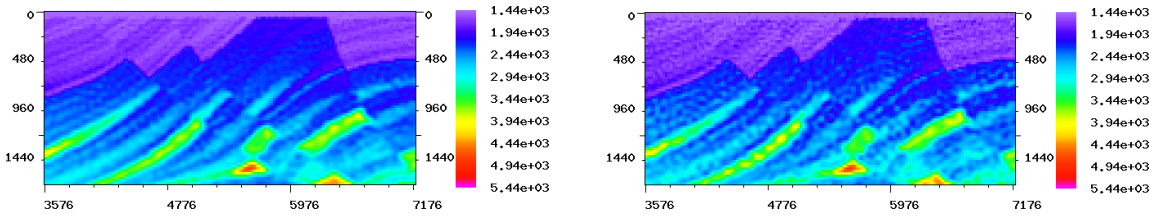

(a) (b)

Figure 3: (a) Target area of the baseline model inverted from a 14 dB SNR synthetic. (b) Target area of the baseline model inverted from a 7 dB SNR synthetic. In both cases the baseline model is reconstructed reasonably well, however, errors due to noise are comparable in magnitude to production-induced effects. [**CR**]

The results of applying cross-updating to the two noisy data sets are shown in Figures 5c and 6c, respectively. The corresponding simultaneous inversion results are shown in Figures 5d and 6d. Since the problem (1) is nonlinear, supplying the result of the highest frequency inversion back to the lowest frequency and repeating the whole inversion cycle for all frequencies may result in achieving a better data misfit. In repeated cycles, lower-frequency inversions usually terminate earlier but higher frequencies still deliver model updates. For an objective comparison of the joint inversion with the parallel, sequential and double-difference methods, the effects of insufficient iteration count are reduced by performing an extra cycle of baseline and monitor inversion in each of the latter methods (we call this approach "iterated" parallel, sequential and double difference). The results of applying the iterated parallel difference to the two noisy data sets are shown in Figures 5a and 6a. The results for the iterated sequential difference are shown in Figures 5b and 6b. The double-difference inversions are shown in Figures 5e and 6e. The double difference method yields the worst results for noisy data, and this is consistent with earlier tests of the method on noisy data (Asnaashari et al., 2012). The sequential difference delivers consistent improvement over the parallel difference, while the cross-updating delivers a significant improvement over the sequential method. The simultaneous inversion and cross-updating appear to yield similar results where $\mathbf{W} \approx 0$. The results of inverting the model difference from the noise-free synthetic and matching acquisition parameters are not shown as all the methods perform well in this case. Joint inversion, either by cross-updating or simultaneous inversion, demonstrates robustness with regard to uncorrelated noise in the data.

Cross-updating keeps the baseline and monitor data spaces separate, and the method is robust with respect to changes in acquisition geometry and source parameters between surveys. Figure 4(b) demonstrates cross-updating with different surveys. The monitor survey in this case has shot positions shifted by 24 m to the right, with shot and receiver depths now changed to 12 and 20 m, respectively. The new monitor Ricker source peak frequency is changed to 12.1 Hz. To isolate the effects of survey acquisition changes from the effects of random noise, our model difference is inverted from a clean synthetic. The result of Figure 4(b), in good agreement with

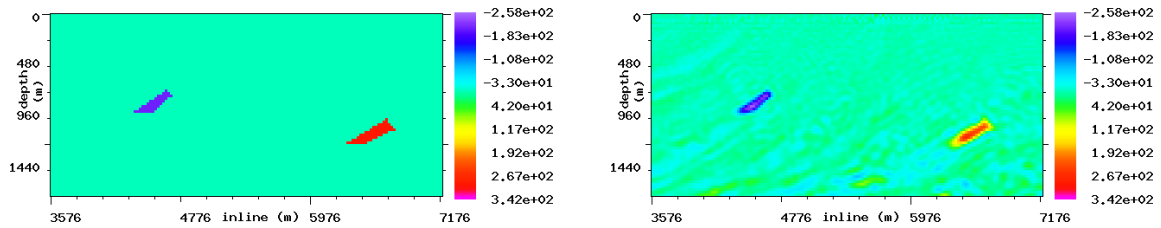

(a) (b)

Figure 4: (a) True velocity difference consists of a negative (−200 m/s) perturbation at about 4.5 km inline 800 m depth, and a positive (300 m/s) perturbation at 6.5 km inline, 1 km depth. (b) Model difference inverted from a clean synthetic for different baseline and monitor acquisition geometries and sources. [**CR**]

the true perturbation of Figure 4(a), demonstrates the robustness of cross-updating with respect to non-random survey repeatability issues.

CONCLUSIONS

Our new simultaneous inversion and cross-updating techniques provide robust alternatives to existing time-lapse FWI methods. Applying the cross-updating method to synthetic data sets with variable amounts of noise achieved a significant reduction of artifacts in the model difference compared to the parallel, sequential, and double difference methods. However, the weighting operator $\mathbf{W}$ in the simultaneous inversion should be chosen using prior knowledge of where production-induced velocity changes are likely to occur. The cross-updating method offers an attractive alternative to the regularized simultaneous inversion as it does not require additional regularization parameters.

In addition to achieving better results than the double difference method for noisy synthetics, cross-updating is less sensitive to repeatability issues that are due to differences in acquisition geometry and sources. The latter may require a cross-equalization of different data vintages (Ayeni and Biondi, 2012) prior to double differencing while the simultaneous inversion and cross-updating do not require data cross-equalization as these methods operate in the model space. However, the simultaneous inversion allows a hybrid approach with a non-zero double-difference term (6) but the practicality of such a combined approach requires further study.

ACKNOWLEDGMENTS

The authors would like to thank Stewart Levin for a number of useful discussions, and the Stanford Center for Computational Earth and Environmental Science for providing computing resources.

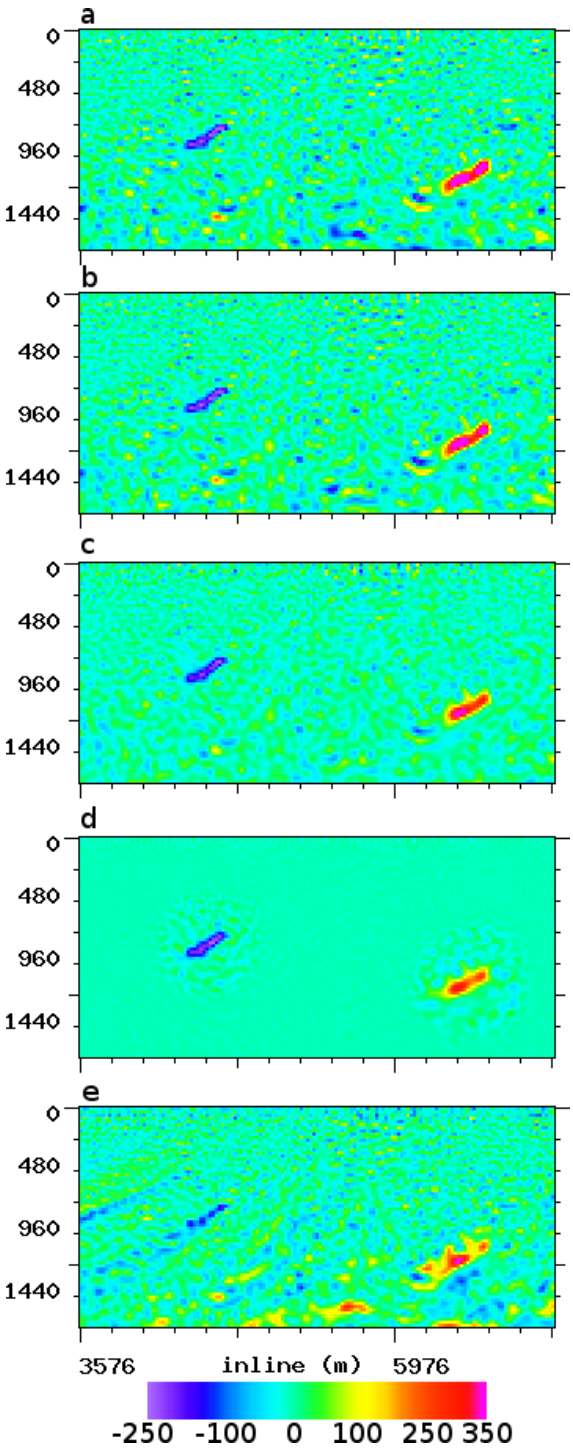

Figure 5: Model difference inverted from a 14 dB SNR synthetic with matching baseline and monitor acquisition geometries using (a) iterated parallel difference; (b) iterated sequential difference; (c) cross-updating; (d) regularized simultaneous inversion; (e) iterated double difference. [**CR**]

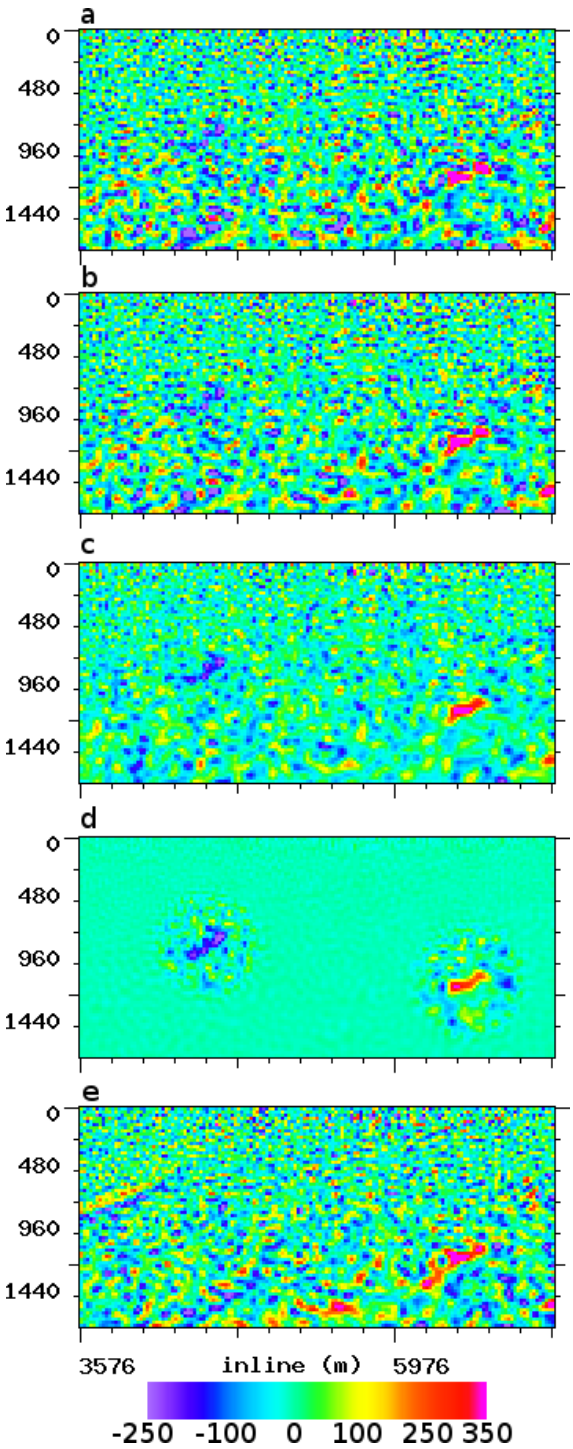

Figure 6: Model difference inverted from a 7 dB SNR synthetic with matching baseline and monitor acquisition geometries using (a) iterated parallel difference; (b) iterated sequential difference; (c) cross-updating; (d) regularized simultaneous inversion; (e) iterated double difference. [**CR**]

REFERENCES

Albertin, U., P. Sava, J. Etgen, and M. Maharramov, 2006, Adjoint wave-equation velocity analysis: 76th Annual International Meeting, SEG, Expanded Abstracts, 3345–3349.

Asnaashari, A., R. Brossier, S. Garambois, F. Audebert, P. Thore, and J. Virieux, 2012, Time-lapse imaging using regularized FWI: A robustness study: 82nd Annual International Meeting, SEG, Expanded Abstracts, doi:10.1190/segam2012-0699.1, 1–5.

Aster, R., B. Borders, and C. Thurber, 2012, Parameter estimation and inverse problems: Elsevier.

Ayeni, G. and B. Biondi, 2012, Time-lapse seismic imaging by linearized joint inversion—A Valhall Field case study: 82nd Annual International Meeting, SEG, Expanded Abstracts, doi:10.1190/segam2012-0903.1, 1–6.

Barkved, O. and T. Kristiansen, 2005, Seismic time-lapse effects and stress changes: Examples from a compacting reservoir: The Leading Edge, **24**, 1244–1248.

Biondi, B., C. Deutsch, R. Gundes, D. Lumley, G. Mavko, T. Mukerji, J. Rickett, and M. Thiele, 1996, Reservoir monitoring: A multidisciplinary feasibility study: 66th Annual International Meeting, SEG, Expanded Abstracts, 1775–1778.

Denli, H. and L. Huang, 2009, Double-difference elastic waveform tomography in the time domain: 79th Annual International Meeting, SEG, Expanded Abstracts, 2302–2306.

Hatchell, P. and S. Bourne, 2005, Measuring reservoir compaction using time-lapse timeshifts: 75th Annual International Meeting, SEG, Expanded Abstracts, 2500–2503.

Maharramov, M. and U. Albertin, 2007, Localized image-difference wave equation tomography: 77th Annual International Meeting, SEG, Expanded Abstracts, 3009–3013.

Maharramov, M. and B. Biondi, 2013, Simultaneous time-lapse full waveform inversion: SEP Report, **150**, 63–70.

Nocedal, J. and S. J. Wright, 2006, Numerical optimization: Springer.

Raknes, E., W. Weibull, and B. Arntsen, 2013, Time-lapse full waveform inversion: Synthetic and real data examples: 83rd Annual International Meeting, SEG, Expanded Abstracts, 944–948.

Routh, P., G. Palacharla, I. Chikichev, and S. Lazaratos, 2012, Full wavefield inversion of time-lapse data for improved imaging and reservoir characterization: 82nd Annual International Meeting, SEG, Expanded Abstracts, doi:10.1190/segam2012-1043.1, 1–6.

Sirgue, L., O. Barkved, J. Dellinger, J. Etgen, U. Albertin, and J. Kommedndal, 2010, Full waveform inversion: the next leap forward in imaging at Valhall: First Break, **28**, 65–70.

Sirgue, L. and R. Pratt, 2004, Efficient waveform inversion and imaging: A strategy for selecting temporal frequencies: Geophysics, **69**, 231–248.

Tarantola, A., 1984, Inversion of seismic reflection data in the acoustic approximation: Geophysics, **49**, 1259–1266.

Virieux, J. and S. Operto, 2009, An overview of full-waveform inversion in exploration geophysics: Geophysics, **74**, no. 6, WCC1–WCC26.

Watanabe, T., S. Shimizu, E. Asakawa, and T. Matsuoka, 2004, Differential waveform tomography for time-lapse crosswell seismic data with application to gas hydrate production monitoring: 74th Annual International Meeting, SEG, Expanded Abstracts, 2323–2326.

Zheng, Y., P. Barton, and S. Singh, 2011, Strategies for elastic full waveform inversion of timelapse ocean bottom cable (OBC) seismic data: 81st Annual International Meeting, SEG, Expanded Abstracts, 4195–4200.